

Sensing characteristics of an optical three-axis tactile sensor under combined loading

Masahiro Ohka*, Yasunaga Mitsuya†, Yasuaki Matsunaga‡ and Shuichi Takeuchi¶

(Received in Final Form: July 28, 2003)

SUMMARY

This paper describes precision enhancement of an optical three-axis tactile sensor capable of detecting both normal force and tangential force. The sensor's single cell consists of a columnar feeler and 2-by-2 conical feelers. We have derived equations to precisely estimate the three-axis force from the area-sum and area-difference of the conical feelers' contact areas by taking into account wrench-length shrinkage caused by a vertical force. To evaluate the equations and determine constants included in the equations, we performed a series of calibration experiments using a manipulator-mounted tactile sensor and a combined load-testing machine. Subsequently, to evaluate the tactile sensor's practicality, it was mounted on the end of a robotic manipulator which rubbed flat specimens such as brass plates with step-heights of $\delta=0.05, 0.1, 0.2$ mm and a brass plate with no step-height. We showed from the experimental data that the optical three-axis tactile sensor can detect not only the step-heights but also the distribution of the coefficient of friction, and that the sensor can detect fine plate inclination with accuracy to about $\pm 0.4^\circ$.

KEYWORDS: Tactile sensor; Optical measurement; Three-axis cell; Combined loading; Surface condition.

1. INTRODUCTION

To date, a variety of tactile sensors have been presented on the basis of various principles, such as variation in electrical capacity and resistance, and piezoelectric and magnetic effects etc.^{1–7} They have played an important role in sensing the friction coefficient⁸ or an object's surface condition.⁹ In particular, the tactile sensor has attracted the greatest anticipation for improving manipulation because a robot must detect the distribution not only of normal force, but also of tangential force applied to its finger surfaces.¹⁰ Material and stability recognition capabilities are advantages of a robotic hand equipped with the three-axis tactile sensor.¹¹ Also, in pig-in-hole, a robot can compensate for its lack of degrees of freedom with the optimum grasping force, allowing an object to move between two fingers using

a measured shearing force occurring on the finger surfaces.¹²

Several designs of the three-axis force cell have been reported using magnetic effects,² variations in electrical capacity,^{4,5} piezoelectric PVDF film⁶ and a photointerrupter.¹² Since constitution of the three-axis force cell is more complicated than that of single-axis force cell, it is difficult to develop a three-axis tactile sensor composed of many three-axis force cells. Consequently, the number of elements in the aforementioned three-axis tactile sensor was insufficient for acquiring the spatial distribution of tactile information. However, if single-crystal silicon is used as the tactile sensor's material, it is relatively easy to produce a complex three-axis force cell structure using semiconductor processing and micro-machining technologies. Therefore, a unique three-axis tactile sensor was composed of many three-axis force cells made of single-crystal silicon elastic rings.¹⁰ Even for single-crystal silicon sensors, however, two principal defects continue to be exhibited: specifically, poor mechanical strength and a slippery surface because they are made of fragile and hard single-crystal silicon.

In contrast, a tactile sensor equipped with an optical waveguide plate has an inherent resistance to mechanical shocks and adapts itself well to the surface of a hard object because its sensing elements are made of soft rubber.^{13–15} This type of tactile sensor comprises the optical waveguide plate, which is made of acrylic and is illuminated along its edge by a light source. The light directed into the plate remains within it due to the total internal reflection generated, since the plate is surrounded by air having a lower refractive index than the plate. The plate maintains contact with the surface of a rubber sheet because a whole array of conical feelers can be attached to the surface of the sheet. If an object maintains contact with the rubber sheet resulting in contact pressure, the feelers collapse. At the contact areas, light is diffusely reflected out of the reverse surface of the plate because the rubber has a higher refractive index than the plate. The distribution of contact pressure is calculated from the bright areas that are viewed from the reverse surface of the plate.

We improved the tactile sensor equipped with this optical waveguide plate to detect the distribution of the three-axis force components,¹⁶ because the conical feelers on the rubber are easily produced by injecting rubber into a mold that features fine concaves formed by precision machining. The present sensor consists of two types of feeler arrays attached to the opposite sides of a rubber sheet. One is a sparse array of columnar feelers that makes initial contact

* Graduate School of Information Science, Nagoya University, Furo-cho, Chikusa-ku, Nagoya, 464-8601 (Japan).

† Graduate School of Engineering, Nagoya University, Furo-cho, Chikusa-ku, Nagoya, 464-8601 (Japan).

‡ Denso, Co. (Japan).

¶ Tokai Rika Denki Co. Ltd. (Japan).

with the object to be recognized. The other is a dense array of conical feelers that maintain contact with the waveguide plate, and each columnar feeler is arranged 2-by-2 with conical feelers, so that it presses against four conical feelers under an applied force. The four contact areas of the conical feelers identify the three force vector components. In our previous paper, we concluded that the optical three-axis tactile sensor separately detected three components of the applied force vector. However, sensitivity to the tangential force varied according to the normal force's magnitude. This defect should be corrected so that this sensor can be applied to a robotic manipulator, which examines an object surface to determine the shape and the surface condition.

In this study, we attempt to enhance the optical tactile sensor's precision and evaluate its applicability for a robotic manipulator. First of all, a model comprising beams was introduced to analyze the variation in tangential sensitivity. While analyzing the model, we discovered that the tangential sensitivity variation resulted from shortening the wrench length of the columnar feeler. Taking that variation into account, we derived equations to precisely estimate the three-axis force from the area-sum and area-difference of the conical feelers' contact areas. Constants included in the equation were determined by a series of calibration experiments using a manipulator-mounted tactile sensor and a combined load testing system. Subsequently, in order to evaluate the practicality of the optical three-axis tactile sensor, it was mounted on the end of a robotic manipulator. The robotic manipulator touched flat specimens, such as plates, having various step-heights ranging from 0.05 to 0.2 mm and a flat plate whose inclination could be varied between -0.38° and 0.38° . From the experimental results, we evaluated the sensing capability for the coefficient of friction, step-height magnitude and inclination of the flat plate.

2. SENSING PRINCIPLE

The schematic view shown in Figure 1 demonstrates the structure of the present sensor. This sensor consists of a rubber sheet, an acrylic plate, a CCD camera (Cony Electronics Co., CN602) and a light source. Two arrays of

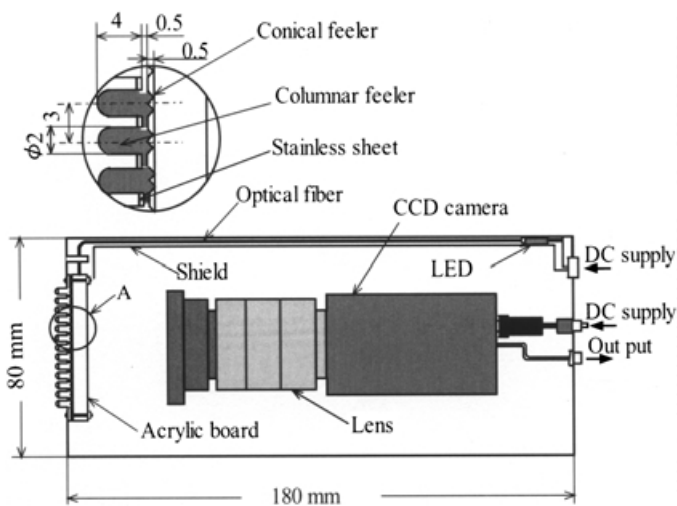


Fig. 1. Schematic of the optical three-axis tactile sensor.

columnar feelers and conical feelers are attached to the detecting surface and the reverse surface of the sensor, respectively. The conical feelers and columnar feelers are made of silicon rubber (Shin-Etsu Silicon Co., KE1404 and KE119, respectively). Their Young's moduli are 0.62 and 3.1 MPa, respectively.

As is evident from Figure 2(a), which illustrates a 3-D view of a single sensing element, four conical feelers are arranged at the bottom of each columnar feeler. If F_x , F_y and F_z are applied to press against these four conical feelers, the vertices of the conical feelers collapse as shown in Figure 2(b). In the previous paper, we derived that the F_x , F_y and F_z were proportional to the x -directional area-difference, A_x , the y -directional area-difference, A_y , and the area-sum, A_z respectively. The parameters A_x , A_y , and A_z are defined below.

$$A_x = S_1 - S_2 - S_3 + S_4 \quad (1)$$

$$A_y = S_1 + S_2 - S_3 - S_4 \quad (2)$$

$$A_z = S_1 + S_2 + S_3 + S_4 \quad (3)$$

Under a combined force, the conical feelers are compressed by the vertical component of the applied force and each cone height shrinks. Consequently, the moment of inertia of the arm length decreases while the normal force increases. Therefore, the relationship between the area-difference and the tangential force should be modified according to the area-sum.

A mechanical model of the single sensing element illustrated in Figure 2(a) has been made to obtain a structure comprising beam elements, shown in Figure 3. Let us assume that in the model, the thick beams supporting four conical feelers have sufficient rigidity because the conical feelers are located under the columnar feeler. Strictly speaking, shearing forces, F_f applied to the tips of four conical feelers are different in proportion to the wrench length of the conical feeler's height. In the present analysis, it is presumed that they are equal because there is no torque with respect to the columnar feeler and the difference in conical feeler's heights is presumed to be relatively small within 20% of the initial height.

In the actual tactile sensor, the columnar feeler is supported by a hole of a stainless steel sheet. The diameter of the holes is slightly larger than that of the columnar feelers, and silicon rubber is molded into the gap between the columnar feeler and the hole; therefore the columnar feelers are not restricted around both x and y axes. We assume there is support by springs of equivalent spring constant K , as shown in Figure 3. The reaction force R generated in the spring should be obtained in the following formulation.

First of all, let us derive the x -directional component R_x of vector R . Since the beam problem shown in Figure 3 is a statically indeterminate structure, it includes unknown reactions that cannot be determined from force and moment equilibrium equations. To solve the statically indeterminate structure, we are attempting to superpose solutions derived from simple statically determinate beams in Figures 4(a) and (b), which are familiar with respect to strength of material. Although the structure in Figure 3 includes conical

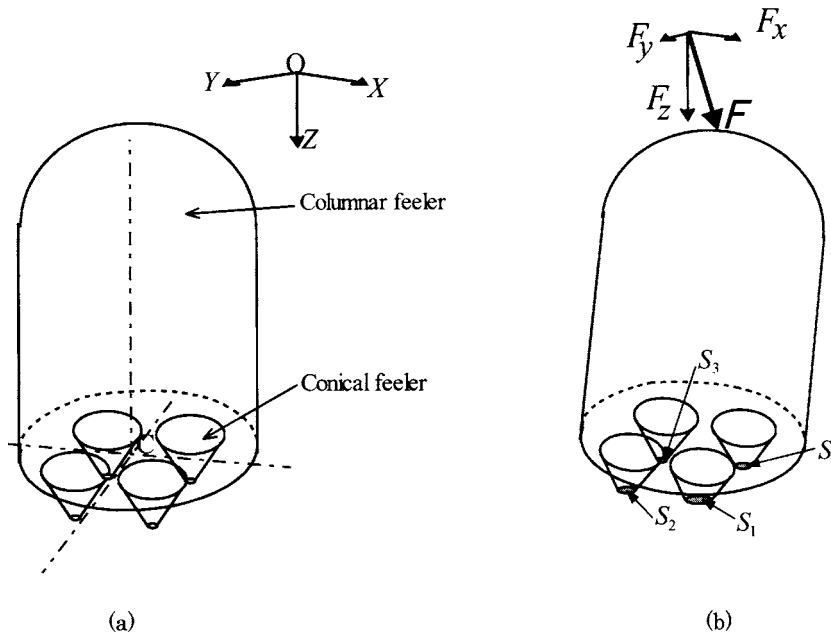


Fig. 2. 3-D view of a columnar feeler and conical feelers. (a) Initial, no force applied. (b) After force has been applied.

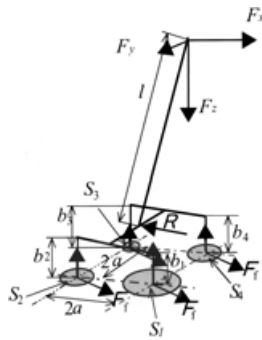
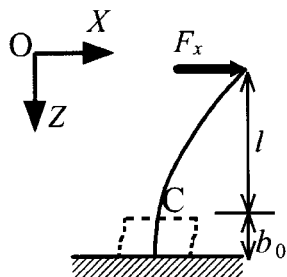


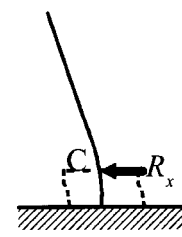
Fig. 3. Beam model.

feelers, a cantilever shown in Figures 4(a) and (b) is assumed for simplification. In Figures 4(a) and (b), we do not consider the deformation of conical feelers because of their aforementioned relatively small degree of deformation. In Figure 4(a), x_1 's directional displacement x_1 is calculated by the following:

$$x_1 = \frac{b_0^3}{3EI} \left(1 + \frac{3l}{2b_0} \right) F_x, \quad (4)$$



(a)



(b)

Fig. 4. Combination of determinate beams. (a) Cantilever loaded at the end point. (b) Cantilever loaded at the intermediate point.

where E and I are Young's modulus and second moment of area, respectively.

Next, x_2 's directional displacement of point C in Figure 4(b) is

$$x_2 = -\frac{R_x b_0^3}{3EI}. \quad (5)$$

On the other hand, R_x is obtained by multiplying the equivalent spring constant K and the resultant displacement of Figures 4(a) and (b). That is,

$$R_x = K(x_1 + x_2). \quad (6)$$

We obtain R_x by substituting Equations (4) and (5) into Equation (6):

$$R_x = \frac{Kb_0^3 \left(1 + \frac{3l}{2b_0} \right)}{3 + \frac{Kb_0^3}{EI}} F_x \equiv \gamma \left(1 + \frac{3l}{2b_0} \right) F_x, \quad (7)$$

where

$$\gamma = \frac{Kb_0^3}{EI} \bigg/ \left(3 + \frac{Kb_0^3}{EI} \right). \quad (8)$$

From equilibrium of force in the z -direction,

$$\begin{aligned} F_z - \alpha_v(S_1 + S_2 + S_3 + S_4) &= 0 \\ F_z &= \alpha_v A_z \end{aligned} \quad (9)$$

is obtained, where α_v is a conversion factor from area to force.

Next, by taking into account variations in a conical feeler's height,

$$b_i = b_0 - \alpha_v S_i / k, \quad (i=1, 2, 3, 4), \quad (10)$$

the equilibrium of moment around the y -axis is obtained. In Equation (10), k is the spring constant of a conical feeler.

$$\begin{aligned} F_x l - (F_f)_x \{ (b_0 - \alpha_v S_1 / k) + (b_0 - \alpha_v S_2 / k) + (b_0 - \alpha_v S_3 / k) \\ + (b_0 - \alpha_v S_4 / k) \} - \alpha_v a (S_1 + S_3) + \alpha_v a (S_2 + S_4) &= 0 \\ F_x l - (F_f)_x (4b_0 - \alpha_v A_z / k) &= \alpha_v a A_x \end{aligned} \quad (11)$$

where $(F_f)_x$ is the x -directional component of the friction force. From the equilibrium of force in the x -direction,

$$F_x + 4(F_f)_x = R_x \quad (12)$$

is obtained. By substituting Equation (7) into Equation (12), the following equation is derived.

$$(F_f)_x = \frac{1}{4} \left\{ \left(\frac{3l}{2b_0} + 1 \right) \gamma - 1 \right\} F_x \quad (13)$$

Substituting Equation (13) into Equation (11),

$$\begin{aligned} F_x l - \frac{1}{4} \left\{ \left(\frac{3l}{2b_0} + 1 \right) \gamma - 1 \right\} (4b_0 - \alpha_v A_z / k) F_x &= \alpha_v a A_x \\ F_x &= \alpha_v a A_x / \left\{ \left(1 - \frac{3}{2} \gamma \right) l + b_0 + \frac{\alpha_v}{4k} \left(\frac{3l}{2b_0} \gamma - 1 \right) A_z \right\} \\ &= \frac{\alpha_v a A_x}{\left(1 - \frac{3}{2} \gamma \right) l + b_0} \left[1 + \frac{\frac{1}{4} \left(\frac{3l}{2b_0} \gamma - 1 \right) \alpha_v A_z}{\left(1 - \frac{3}{2} \gamma \right) l + b_0} \right]^{-1} \end{aligned} \quad (14)$$

Since $\alpha_v A_z / k$ represents the compressive displacement of a conical feeler's height, the value is 0.1 mm in the case of 20% strain in the height direction. Substituting dimensions of the present sensing elements and material constants into Equation (14), the second term in the bracket becomes approximately 0.002, and is negligibly small compared to 1. If an approximate expression $(1 + \varepsilon)^{-1} \cong 1 - \varepsilon$ is applied to Equation (14), then

$$\begin{aligned} F_x &\cong \left[\alpha_v a \left\{ \left(1 - \frac{3}{2} \gamma \right) l + b_0 \right\}^{-1} - \frac{\alpha_v^2 a}{4k} \left\{ \left(1 - \frac{3}{2} \gamma \right) l + b_0 \right\}^{-2} \right. \\ &\quad \left. \times \left(\frac{3l}{2b_0} \gamma - 1 \right) A_z \right] A_x \end{aligned} \quad (15)$$

Therefore,

$$F_x = (\alpha_{h0} - \alpha_h A_z) A_x, \quad (16)$$

where α_{h0} and α_h are coefficients of A_x and $A_z A_x$, respectively.

Applying same procedure as the aforementioned to the equilibrium of moment around the x -axis, we derive

$$F_y = (\alpha_{h0} - \alpha_h A_z) A_y, \quad (17)$$

Consequently, we obtain

$$\begin{aligned} F_x &= (\alpha_{h0} - \alpha_h A_z) A_x \\ F_y &= (\alpha_{h0} - \alpha_h A_z) A_y \\ F_z &= \alpha_v A_z \end{aligned} \quad (18)$$

3. ALGORITHM FOR AREA DETECTION

Figure 5 shows the 2-by-2 contact areas of conical feelers that are located on the reverse side of a columnar feeler. The mesh indicates CCD camera pixels, and the hatched portions of the mesh show the contact areas. If we multiply the number of hatched portions by the pixel area, we can obtain the contact area's dimensions. The hatched portions are counted in the four quadrangles denoted by thick solid lines to obtain S_1 , S_2 , S_3 and S_4 which are included in Equations (1), (2) and (3). We call the region of the four quadrangles "quadrisection region" in the following.

The positions of the conical feeler's tips should be measured to identify the quadrisection regions. In this paper, histograms of pixel numbers exceeding a proper threshold are obtained for both vertical and horizontal directions. The positions of the conical feeler's tips are determined from the positions of the histogram vertices. Next, we present the procedure to identify the quadrisection region. In this procedure, a 4-by-3 sensor is used as an example. The horizontal and vertical axes of the image are denoted by i and j , respectively, and the gray scale value at (i, j) is denoted by $g(i, j)$. The axes of i and j are aligned to coincide with the axes of the pixel coordinate system on the CCD.

[Step 1]. A flat object is kept in contact with the whole sensor surface and the gray scale image is acquired (Figure

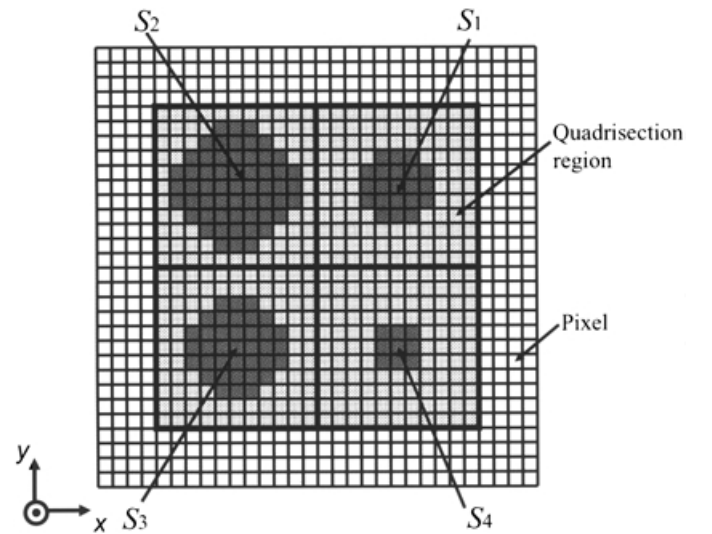


Fig. 5. Schematic view for explaining definition of quadrisection region and estimation of four contact areas.

6(a). The gray scale image is transformed into a binary image by applying a proper threshold, T :

$$b(i, j) = \begin{cases} 1, & (g(i, j) > T) \\ 0, & (g(i, j) \leq T) \end{cases} \quad (19)$$

[Step 2]. The histogram of pixels satisfying $b(i, j) = 1$ is obtained for the i -direction. The histogram $f(i)$ is calculated by

$$f(i) = \sum_{j=1}^N b(i, j), \quad (20)$$

where N is the total number of pixels in the j -direction. Figure 6(b) illustrates the relationship between $f(i)$ and i .

[Step 3]. The distribution of $f(i)$ is quantized using the threshold cf_{\max} denoted by the solid line in Figure 6(b).

$$\hat{f}(i) = \begin{cases} 1, & (f(i) > cf_{\max}) \\ 0, & (f(i) \leq cf_{\max}) \end{cases} \quad (21)$$

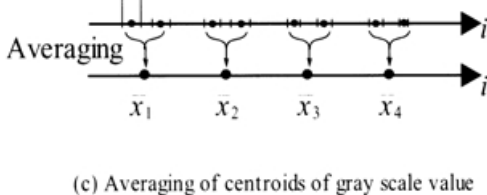
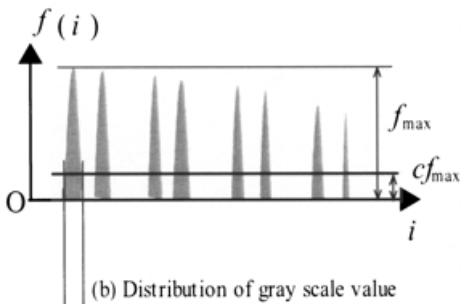
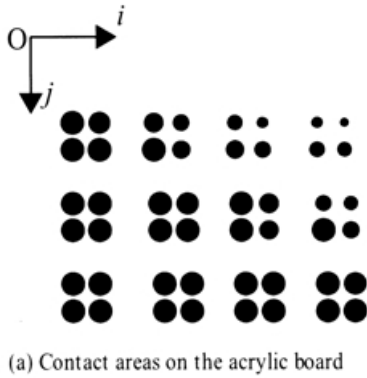
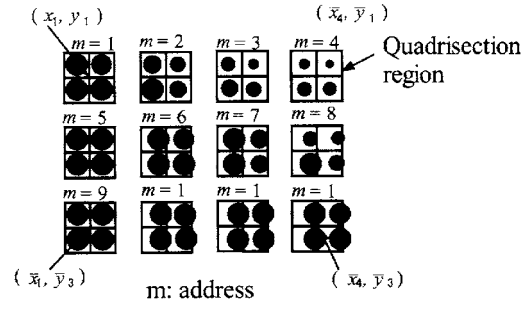
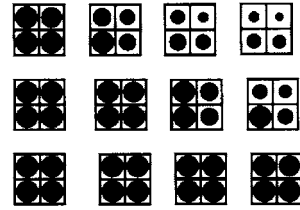


Fig. 6. Identification of the quadrisection regions.



(a) before modification of lens aberration



(b) after modification

Fig. 7. Modification of the quadrisection region.

Here, c is the appropriate constant.

[Step 4]. The adjacent regions satisfying $\hat{f}(i) = 1$ are paired. The center of gravity is calculated for each region, and mean gravity centers, \bar{x}_k ($k=1 \sim 4$), are obtained for each pair as shown in Figure 6(c).

[Step 5]. Mean gravity centers in the j -direction, \bar{y}_l ($l=1 \sim 3$) are calculated by performing Steps 2~4 for the j -direction.

[Step 6]. The quadrisection regions are specified by the coordinates (\bar{x}_k, \bar{y}_l) , as shown in Figure 7(a).

[Step 7]. Since the image is warped by the lens aberration of the CCD camera, the quadrisection regions obtained in Step 6 are modified as shown in Figure 7(b). In this modification, the actual (\bar{x}_k, \bar{y}_l) is determined by four conical feeler centers, which is the nearest quadrisection region obtained in Step 6.

4. CALIBRATION TESTS

4.1. Experimental procedure

To calibrate constants included in Equation (18), combined forces were applied to the tip of a columnar feeler. The tip displacement was measured with a micrometer and a pulse motor mounted on an X-Z stage. The generated force was measured by a three-axis force sensor (Nitta Co., TFS-2012A05). We performed calibration tests A and B as follows.

[Calibration test A] A normal force was applied to the tip of the columnar feeler to obtain the relationship between area-sum, A_z and normal force, F_z . To verify homogeneity of the sensor cells' sensitivity, we performed this procedure on three different columnar feelers.

[Calibration test B] Under a constant normal force, F_{z0} , a tangential force was applied to the tip of the columnar feeler

to obtain the relationship between area-difference, A_x and tangential force, F_x . We varied the normal force level to obtain several curves for A_x versus F_z under different normal forces.

4.2. Experimental results and discussion

Figure 8 shows A_z versus F_z for calibration test A. Three different symbols indicate at three columnar feelers located at different addresses. As shown in Figure 8, the relationships between A_z and F_z are almost linear and the three results coincide with each other. These results indicate that the z -directional sensitivity is calculated by Equation (18)₃, assuming a linear relationship between A_z and F_z , and that the z -directional sensitivity does not depend on the address of the columnar feeler. From the results, we obtain the value of the constant α_v , included in Equation (18)₃.

Next, let us discuss the x -directional sensitivity obtained by calibration test B. The relationship between the area-difference, A_x and the x -directional force, F_x is shown in Figure 9. The solid line in this figure shows the estimation obtained from the method of least squares. We performed several similar experiments with different values of the constant normal force, F_{z0} . Variation in $\alpha_{h0} - \alpha_h A_z (\equiv \alpha_l)$ obtained from these results is shown in Figure 10. From this diagram, we obtained the constants α_{h0} and α_h included in Equation (18)₁. From the above-mentioned calibration tests

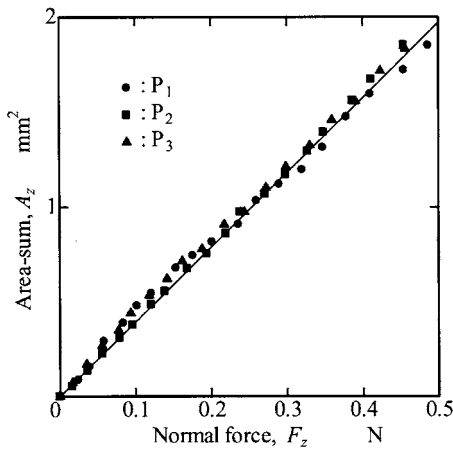


Fig. 8. z -directional sensitivity (Experiment A).

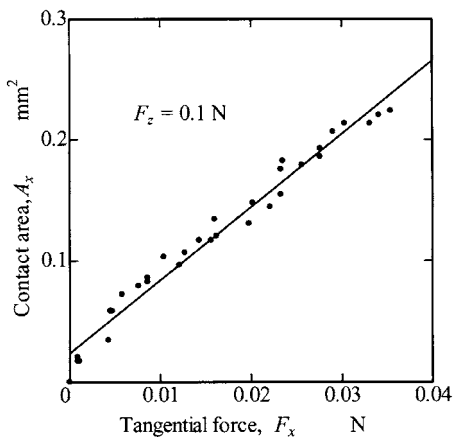


Fig. 9. x -directional sensitivity (Experiment B).

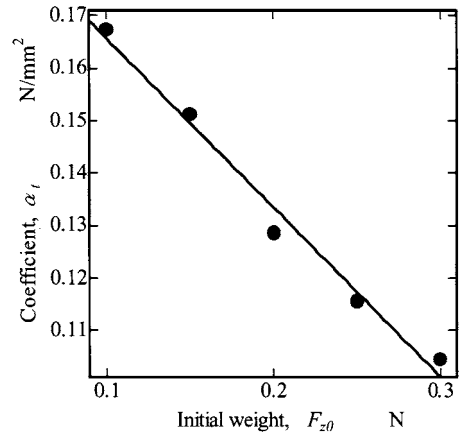


Fig. 10. Estimation of α_{h0} and α_h (Experiment B).

A and B, we identified values of the constants $\alpha_v=0.25 \text{ N/mm}^2$, $\alpha_{h0}=0.20 \text{ N/mm}^2$ and $\alpha_h=0.081 \text{ N/mm}^4$.

5. STEP-HEIGHT DETECTION

5.1. Experimental procedure

The present sensor was mounted on a manipulator with five degrees of freedom as shown in Figure 11, and the robot rubbed a brass plate with the tactile sensor. We prepared three brass plates with step-heights of $\delta=0.05, 0.1, 0.2 \text{ mm}$, and a brass plate with no step-height ($\delta=0 \text{ mm}$) as shown in Figure 12. In this experiment, the robot rubbed the brass plates to find the best parameter for distinguishing between

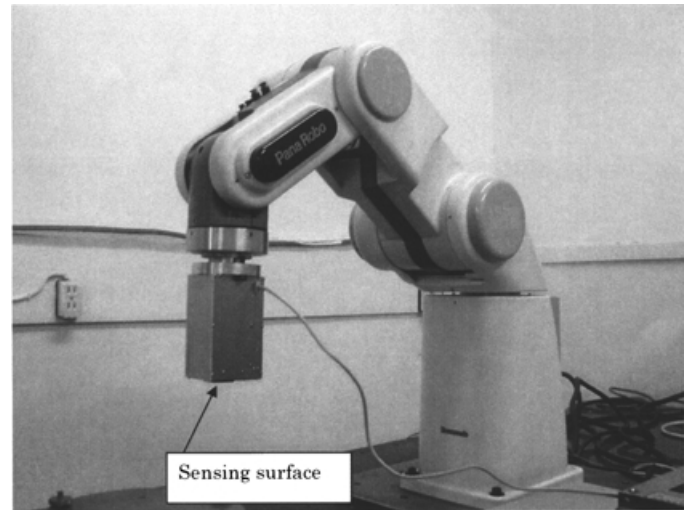


Fig. 11. Robot equipped with the three-axis tactile sensor.

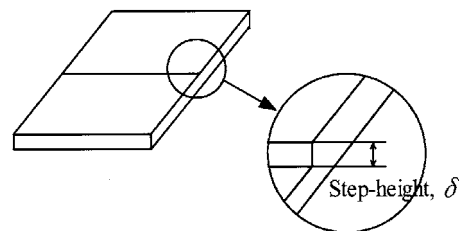


Fig. 12. Specimen having step-height.

step-heights, and to examine its ability to distinguish between step-heights.

5.2. Experimental results and discussion

We selected the best parameter to display the step-height profile. The robotic manipulator brushed against the brass plate with step-height $\delta=0.1$ mm to obtain the experimental results shown in Figure 13. Figures 13(a), (b) and (c) show variations in F_z , F_x and the friction coefficient, μ , respectively. The abscissa of each figure is the horizontal displacement of the robotic manipulator. As shown in these figures, F_z and F_x jump at the step-height position. Although these parameters are convenient for presenting the step-height, the variation in F_z is better than that in F_x because it does not have a concave portion, which does not exist on the brass surface. Therefore in the next figure, F_z is adopted as the parameter to represent step-height. It is noted that variation in the friction coefficient, μ , is almost flat while

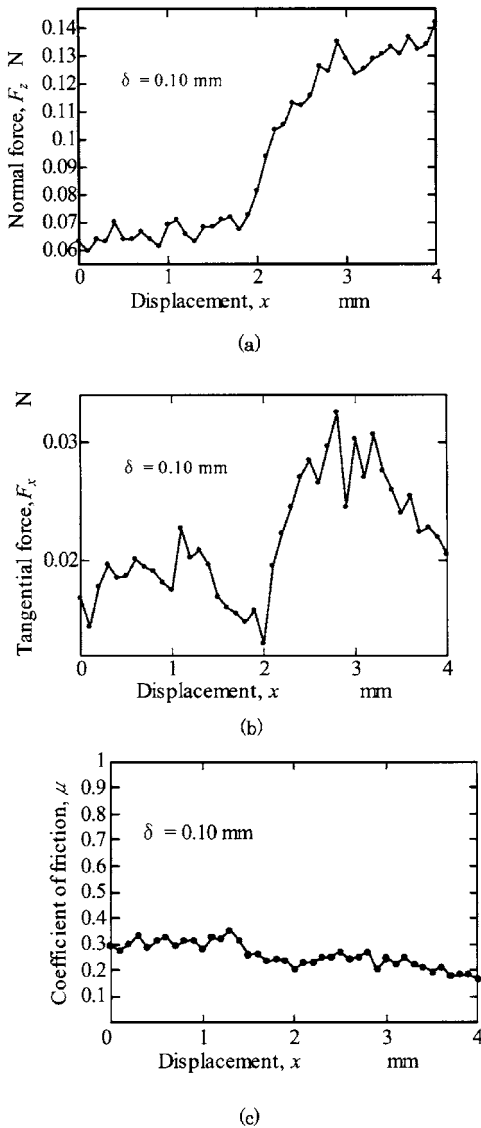


Fig. 13. Estimation of the best parameter for step-height presentation. (a) Normal force, F_z . (b) Tangential force, F_x . (c) Coefficient of friction, μ .

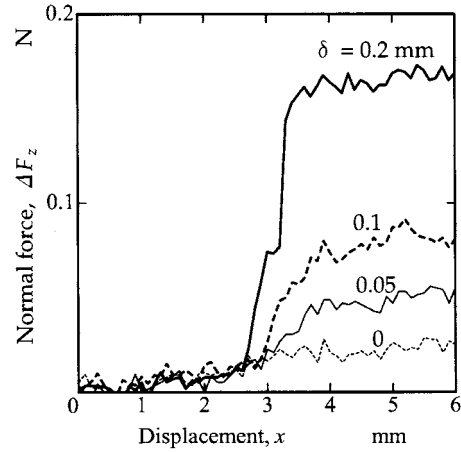


Fig. 14. Step-height detection (Going up the step).

the robot was rubbing the tactile sensor on the brass plate at the step-height. This indicates that the tactile sensor can detect the distribution of the coefficient of friction because that coefficient should be uniform over the entire surface.

Figure 14 shows detection results for step-heights of $\delta=0.05$, 0.1 and 0.2 mm. The ordinate of Figure 14 is variation in the vertical force from the initial vertical force, $\Delta F_z = F_z - F_{z0}$. As evident from Figure 14, experimental results vary according to the step; if the step-height magnitudes of the experimental results are examined, it is found that the ratio is about 1:2:5, and that the ratio approximates the ratio of the step-heights formed on the brass plates (1:2:4). Therefore, the sensor can detect step-heights formed on the surface of an object.

While the aforementioned results are for step climbing, Figure 15 shows detection results for step-heights when descending the steps. Figures 14 and 15 show that the variation in ΔF_z corresponds to the step-height value. Therefore, from the results shown in Figures 14 and 15, we conclude that the present sensor can detect the step-height value regardless of the direction of movement. In addition, we found from a comparison of Figures 14 and 15 that the normal force detection exhibits some hysteresis. This hysteresis appears to be caused by slippage of conical feelers' tips induced by a tangential force exceeding the maximum static friction force between the conical feelers

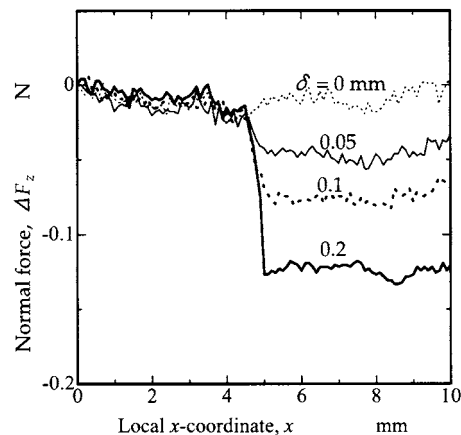


Fig. 15. Step-height detection (Going down the step).

and the acrylic board. This suggests that some improvement has been made to the present sensing element.

6. INCLINATION DETECTION

6.1. Experimental procedure

The present tactile sensor is able to detect inclination of a flat object by inhomogeneously distributing pressure caused by contact. In the experiment, the robotic manipulator touches the flat plate whose inclination is adjusted with three fine screws. Angles of the sensing surface from the specimen surface are varied between -0.38° and 0.38° .

6.2. Experimental results and discussion

The vertical displacement of the columnar feeler's tip U_z is calculated using the spring coefficient of the conical feeler, k . Since a columnar feeler is supported by four conical feelers, displacement in the z -direction, U_z is calculated by F_z and the resultant spring constant $k_v (=4k)$ as follows:

$$U_z = \frac{\alpha_v}{k_v} A_z. \quad (22)$$

In order to determine the constant k_v , coefficient $\alpha_v/k_v = 0.26$ l/mm was obtained from the relationship between vertical displacement and the area-sum. If $\alpha_v = 0.25$ N/mm² obtained in Section 4.2 is substituted into $\alpha_v/k_v = 0.26$ l/mm, $k_v = 0.96$ N/mm is obtained.

Variations in U_z of three continuously aligned sensing elements are shown in Figure 16. Figures 16(a), (b), (c), (d) and (e) show results of specimen inclinations of 0.38° , 0.19° , 0 , -0.19° and -0.38° , respectively. As shown in Figure 16(c) (case where $\theta = 0^\circ$), outputs of three sensing elements closely agree. However, differences among the three outputs increase as the magnitude of θ increases.

The aforementioned result indicates that vertical displacements of three continuously aligned sensing elements estimate the fine inclination of the plate. To quantitatively determine the inclination, the mean value of differences between outputs of two adjacent sensing elements m is obtained, and it is divided with distance between two adjacent sensing elements, d to obtain inclination of the plate, Θ calculated by the expression, $\Theta = \tan^{-1}(m/d)$. We obtained Θ with the aforementioned procedure shown in Figure 17. We found that applied inclination of the plate agrees with the calculated inclination Θ with outputs of three sensing elements. Therefore, fine inclination of the plate can be evaluated by Θ .

7. CONCLUSION

We developed an optical three-axis tactile sensor and mounted it on the wrist of a robot so that the robot could detect an object's surface condition. We derived equations to precisely estimate the three-axis force from the area-sum and area-difference of conical feelers' contact areas, and developed a procedure to determine those contact areas.

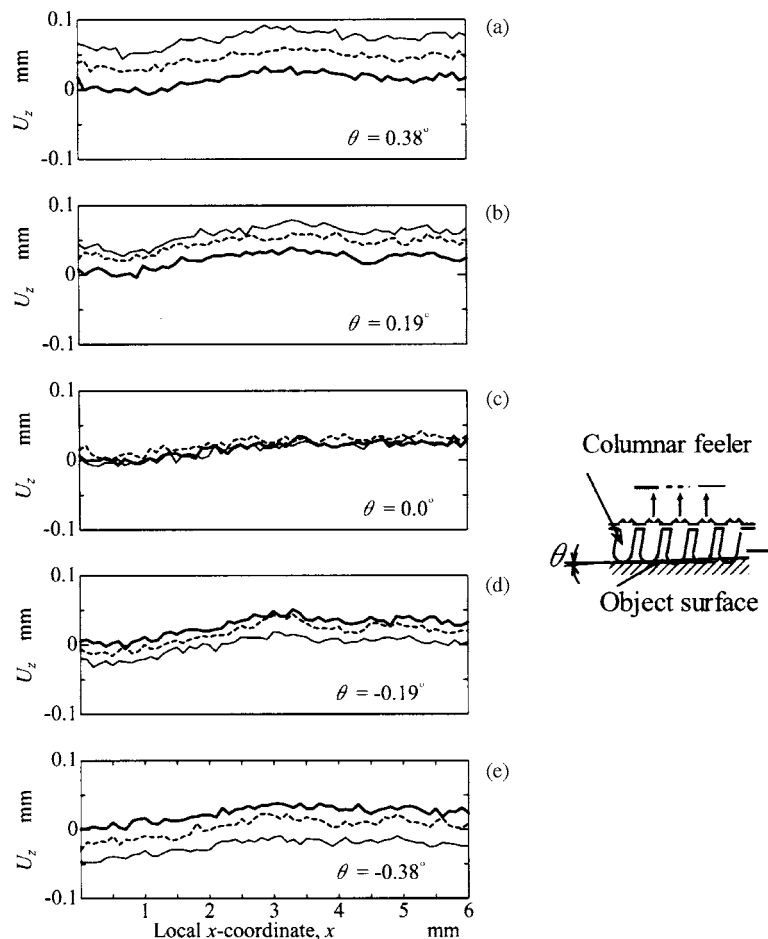


Fig. 16. Outputs of three sequential feelers under inclination detection.

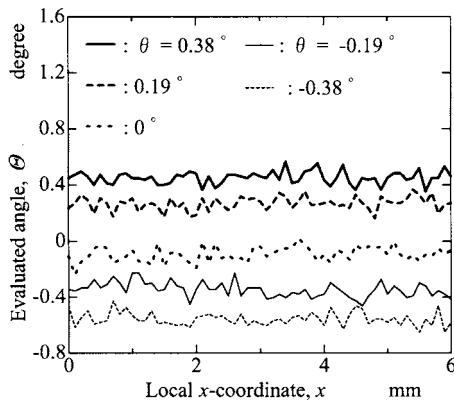


Fig. 17. Evaluated inclination.

Constants included in the equations were determined by a series of calibration experiments. Subsequently, to evaluate practicality of the optical three-axis tactile sensor, the robotic manipulator touched flat specimens such as plates having various step-heights ranging from 0.05 to 0.2 mm and a flat plate whose inclination could be varied between -0.38° and 0.38° . Experimental results show that the optical three-axis tactile sensor can detect not only the step-heights, but also the distribution of the coefficient of friction, and that the present tactile sensor can detect fine plate inclination with an accuracy of about $\pm 0.4^\circ$.

References

1. H.M. Raibert and J.E. Tanner, "Design and Implementation of a VSLI Tactile Sensing Computer," *Int. J. Robotics Res.* **1**(3), 3-18 (1982).
2. S. Hackwood, G. Beni, L.A. Hornak, R. Wolfe and T. Nelson, "Torque-Sensitive Tactile Array for Robotics," *Int. J. Robotics Res.* **2**(2), 46-50 (1983).
3. P. Dario, D.D. Rossi, C. Domenci and R. Francesconi, "Ferroelectric Polymer Tactile Sensors with Anthropomorphic Features," *Proc. 1984 IEEE Int. Conf. on Robotics and Automation* (1984) pp. 332-340.
4. J.L. Novak, "Initial Design and Analysis of a Capacitive Sensor for Shear and Normal Force Measurement," *Proc. of*

- 1989 IEEE Int. Conf. on Robotic and Automation* (1989) pp. 137-145.
5. M. Hakozaki and H. Shinoda, "Digital Tactile Sensing Elements Communicating Through Conductive Skin Layers," *Proc. of 2002 IEEE Int. Conf. on Robotics and Automation* (2002) pp. 3813-3817.
6. Y. Yamada and R. Cutkosky, "Tactile Sensor with 3-Axis Force and Vibration Sensing Function and Its Application to Detect Rotational Slip," *Proc. of 1994 IEEE Int. Conf. on Robotics and Automation* (1994) pp. 3550-3557.
7. H.R. Nicholls and M.H. Lee, "A Survey of Robot Tactile Sensing Technology," *Int. J. Robotics Res.* **8**(3), 3-30 (1980).
8. A. Bicchi, J.K. Salisbury and P. Dario, "Augmentation of Grasp Robustness Using Intrinsic Tactile Sensing," *Proc. of 1989 IEEE Int. Conf. on Robotics and Automation* (1989) pp. 303-307.
9. R.D. Howe and M.R. Cutkosky, "Dynamic Tactile Sensing: Perception of Fine Surface Features with Stress Rate Sensing," *IEEE Trans on Robotics and Automation* **9**, No. 2, 140-151 (1993).
10. M. Ohka et al., "Tactile Expert System Using a Parallel-fingered Hand Fitted with Three-axis Tactile Sensors," *JSME Int. J., Series C* **37**, No. 1, 138-146 (1994).
11. S. Takouchi, M. Ohka and Y. Mitsuya, "Tactile Recognition Using Fuzzy Production Rules and Fuzzy Relations for Processing Image Data from Three-dimensional Tactile Sensors Mounted on a Robot Hand," *Proc. of the Asian Control Conf.*, 631-634 (1994).
12. B. Borovac, L. Nagy and M. Sabli, "Contact Tasks Realization by Sensing Contact Forces Theory and Practice of Robots and Manipulators," *Proc. of 11th CISM-IFTNN Symposium*, Springer Wien, New York (1996) pp. 381-388.
13. K. Tanie et al., "A High Resolution Tactile Sensor," *Proc. of 4th Int. Conf. on Robot Vision and Sensory Controls* (1984) pp. 251-260.
14. C. Mott et al., "An Experimental Very High Resolution Tactile Sensor Array," *Proc. 4th Int. Conf. on Robot Vision and Sensory Controls* (1984) pp. 241-250.
15. H. Maekawa et al., "Development of Finger-shaped Tactile Sensor and Its Evaluation by Active Touch," *Proc. of the 1992 IEEE Int. Conf. on Robotics and Automation* (1992) pp. 1327-1334.
16. M. Ohka et al., "A Three-axis Optical Tactile Sensor (FEM Contact Analyses and Sensing Experiments Using a Large-sized Tactile Sensor)," *Proc. of the 1995 IEEE Int. Conf. on Robotics and Automation* (1995) pp. 817-824.